analytical chemistry

pubs.acs.org/ac Article

Multiplexed Magnetofluorescent Bioplatform for the Sensitive Detection of SARS-CoV-2 Viral RNA without Nucleic Acid Amplification

Riham Zayani, Dorra Rezig, Wasfi Fares, Mouna Marrakchi, Makram Essafi, and Noureddine Raouafi*

Cite This: *Anal. Chem.* 2021, 93, 11225–11232 Read Online

ACCESS | Metrics & More | Article Recommendations | Supporting Information

ABSTRACT: Rapid and sensitive detection of SARS-CoV-2 virus genetic material is of paramount importance to mitigate the COVID-19 pandemic outbreak and lower the death toll. Herein, we report the design of a magnetofluorescent bioplatform for the direct and specific detection of the viral RNA of SARS-CoV-2 in the total RNA extracted from nasopharyngeal swabs of COVID-19-positive patients. A higher fluorescence response was achieved using two capture probes tethered to magnetic beads using a biotin/streptavidin linkage, targeting two specific sites in the ORF1a and S genes. Two horseradish peroxidase (HRP)-conjugated reporter sequences, complementary to the loci of the S and N genes, were used to reveal the presence of the viral RNA through the oxidation of *o*-phenylenediamine to fluorescent 2,3-diaminophenazine. Under optimal conditions, the bioplatform showed high selectivity and sensitivity and was able to detect as low as 0.01 ng of viral RNA (1×10^3 copies/μL) with a linear dynamic range varying from 0.01 to 3.0 ng (1×10^3 to 9×10^7 copies/μL). The bioplatform was also able to discriminate the SARS-CoV-2 RNA from those of other related viruses such as hepatitis C, West Nile, measles, and non-polio viruses. Furthermore, the developed biosensor was validated in 46 clinical samples (36 COVID-19-positive patients and 10 COVID-19-negative subjects, as assessed with the gold standard RT-qPCR method). Both sensitivity and specificity of the developed method reached 100%. Finally, making such a simple and specific method available in the field, at a primary point of care, can better help the detection of SARS-CoV-2 infection in low-resource settings.

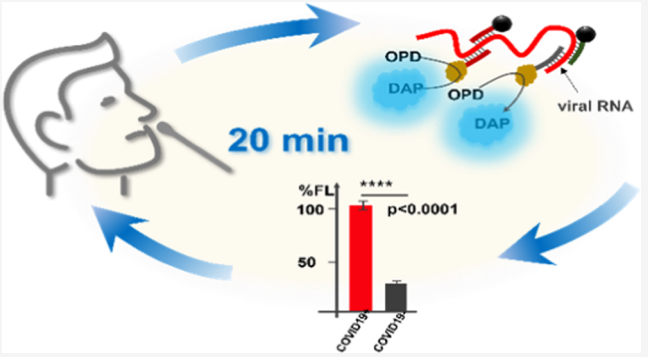

COVID-19 is a global pandemic that started in the Hubei province of China at the end of 2019.[1] To date, nearly 3.2 million lives have been lost and the disease is predicted to persist until next summer and beyond.[2] Worldwide, national authorities took drastic measures to curb the pandemic propagation by implementing lockdowns, restricting social gatherings, and shutting down schools and universities. However, the current situation is still a threat to humanity with the ongoing second and third waves of the pandemic.[3,4] Furthermore, emergent variants with mutations in the receptor-binding domain of the spike protein genes such as D614G[5] and N501Y[6] make the virus more infectious, which will probably cause higher fatalities.[7] Efficient outbreak control will then need cost-effective and easy-to-operate detection tools that can be easily deployed both in industrialized countries and in low-resource settings.[8]

The first wave underpinned the crucial role of diagnostic methods in controlling the pandemic outbreak,[9] which requires massive diagnostic testing to implement the appropriate therapy and taking appropriate measures to prevent further spread of the virus. To date, the U.S. Food and Drug Administration has granted an Emergency Use Authorization for more than 336 COVID-19 tests of which approximately 72% are molecular biology-based tests using polymerase chain reaction (PCR), loop-mediated isothermal amplification (LAMP), transcription-mediated amplification (TMA), selective temperature amplification reaction (STAR), and clustered regularly interspaced short palindromic repeats (CRISPRs), etc.[10,11] Although a large number of publications have reported the detection SARS-CoV-2, those avoiding RNA amplification remain scarce. For instance, Moitra et al. reported a selective naked-eye detection procedure of the viral RNA using plasmonic nanoparticles capped with antisense oligonucleotides targeting the N gene. In the presence of the target, the modified AuNPs agglomerate, inducing a change in localized surface plasmon resonance.[12] Addition of RNaseH cleaves the heterohybrid to form a precipitate visible to the naked eye. The

Received: May 7, 2021
Accepted: July 23, 2021
Published: August 2, 2021

https://doi.org/10.1021/acs.analchem.1c01950
Anal. Chem. 2021, 93, 11225–11232

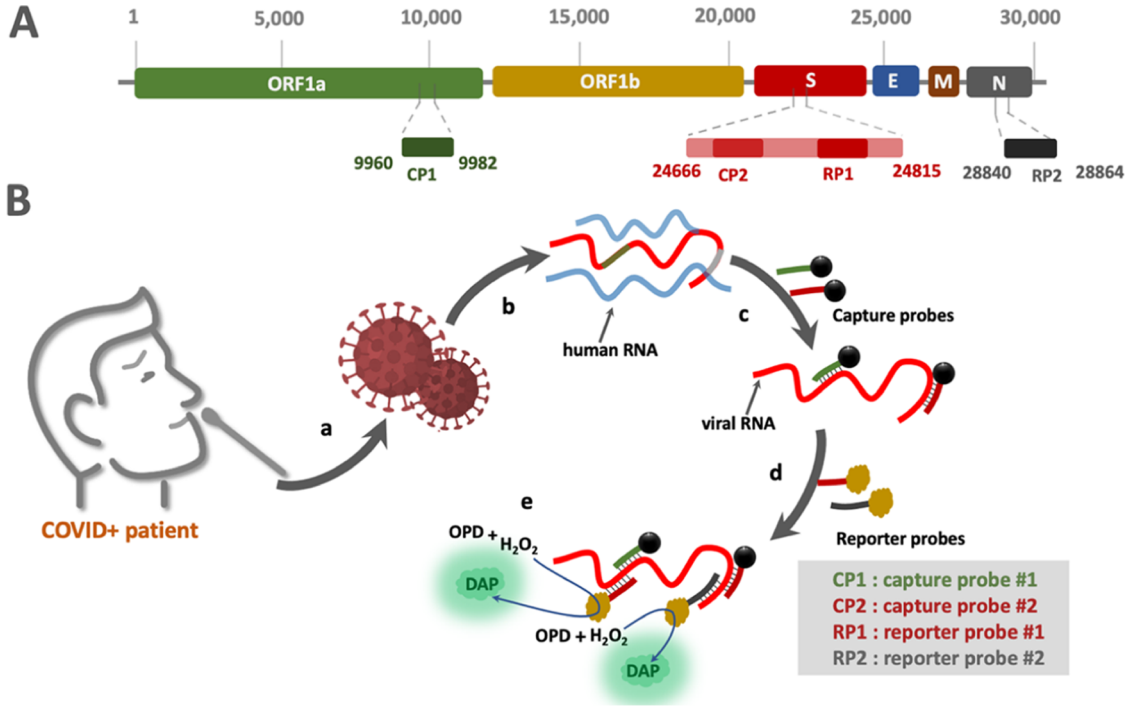

Figure 1. (A) Schematic representation of the structure of total RNA of the SARS-Cov-2 virus with the location of the target sequences on the ORF1a, S, and N genes, chosen to design the capture probe (CP) and the reporter probe (RP) used in this work. (B) Schematic display of the stepwise procedure to capture and detect the viral RNA by means of magnetic probes and HRP-terminated reporters: (a) nasal swabs; (b) extracting the total RNA; (c) adding magnetic capture probes and magnet-mediated purification of the complex; (d) hybridizing with HRP-conjugated reporter probes; and (e) generating HRP-catalyzed fluorescence readout after adding OPD and H_2O_2.

assay is mainly qualitative with a dynamic range varying from 0.2 to 3 ng/μL and a detection limit of 0.18 ng/μL. The main advantage of such an approach is its rapidity since it takes only 10 min to be performed. Alafeef et al. have also reported a sensitive electrochemical paper-based RNA detection method using four specific oligonucleotides to capture RNA on the surface of a graphene-modified paper.[13] The approach was sensitive enough to detect 6.9 copies/μL without going through any RNA amplification step. Moreover, Fozouni et al. reported an amplification-free detection of viral RNA with CRISPR−Cas13a and mobile phone microscopy readout. The assay achieved ∼100 copies/μL in less than 30 min or in 5 min if pre-extracted viral RNA was used.[14] Combining several crRNAs targeting different RNA regions allows substantial improvement in the sensitivity. Lateral flow immunoassays are useful to carry out mass screening for diseases and showed their usefulness in point-of-care COVID-19 detection.[15−17] An amplification-free nucleic acid immunoassay was implemented on a lateral flow strip using fluorescence detection of SARS-CoV-2 RNA with an heterohybrid DNA−RNA antibody and fluorescent nanoparticles. Several DNA probes targeting conserved regions of the open reading frame 1ab (ORF1ab), envelope (E), and nucleocapsid (N) genes were used to improve the bioassay sensitivity.[18] An interesting triple-mode (Raman, fluorescence, and UV) biosensor for direct RNA detection, benefitting from gold nanoparticles as a color-shifting agent and a Raman signal enhancer was reported by Gao et al.[19]

Designing rapid, sensitive, and nucleic acid amplification-free methods for the detection of SARS-CoV-2 could be advantageous to prevent its spread and mitigate the pandemic. Herein, we report a novel method to sensitively and directly detect the viral RNA in total RNA samples collected from nasal swabs of COVID-19-positive patients using a magnetofluorescent bioassay. The latter uses a set of antisense capture and reporter oligonucleotides that recognize specific regions of the viral RNA in ORF1a, S, and N genes. The fluorescence readout is induced by HRP, which oxidizes fluorogenic *o*-phenylenediamine (OPD) to fluorescent 2,3-diaminophenazine (DAP) in the presence of hydrogen peroxide. The assay can detect less than 1.02×10^3 copies/μL in the range from 1×10^3 to 9×10^7 copies/μL in less than 30 min. Moreover, the developed assay was able to specifically recognize the target SARS-CoV-2 RNA, discriminating COVID-19-positive patients from healthy subjects. Selectivity of our device was better verified when challenged with several RNA positive-sense enteroviruses such as HCV, West Nile virus, measles virus, and non-polio enteroviruses. The bioassay was further validated using a cohort of 46 clinical specimens of the total RNA collected from COVID-19-positive patients and healthy subjects (assessed with the gold standard RT-qPCR method), showing a total match with 100% sensitivity and specificity. The schematic representation of the designed assay is depicted in Figure 1.

EXPERIMENTAL SECTION

Materials. Streptavidin-coated magnetic beads (Strep-MBs, 4 mg/mL, 1 μm nonporous superparamagnetic microparticles) were purchased from New England Biolabs (Germany). A horseradish peroxidase (HRP) conjugation kit (ab102890) was purchased from Abcam (U.K.). All of the chemicals, *o*-phenylenediamine (OPD), hydrogen peroxide (37%), NaH_2PO_4, K_2HPO_4, KCl, and KCN, were bought from Sigma-Aldrich (Germany) and were used without further purification. The following buffer solutions, prepared with

https://doi.org/10.1021/acs.analchem.1c01950
Anal. Chem. 2021, 93, 11225−11232

ultrapure water and sterilized after preparation, were used: binding and wash buffer (B&W) (10 mM Tris−HCl, pH 7.5, containing 1 mM EDTA and 2 M NaCl) and saline−sodium citrate (SSC) buffer (30 mM sodium citrate and 500 mM NaCl, pH 7.4). All of the nucleic sequences were prepared in DNase/RNase-free distilled water purchased from Invitrogen. All of the measurements were carried out in phosphate-buffered saline (PBS) solutions prepared in deionized water.

The nucleic acid sequences were synthetized by Biomers GmbH (biomers.net) and are listed in Table S1 of the Supporting Information (SI) file.

RESULTS

Design of the Assay. As shown in Figure 1, which summarizes the development of our approach, the antisense capture probes targeting two separated loci on the virus genetic RNA (ORF1ab and S genes) were chosen to increase the chance of access to the viral RNA. Several recent works opted to target the viral RNA with multiple probes to improve its capture.[12,13,18] In our case, the chosen oligonucleotides were tethered to commercial streptavidin-coated magnetic beads owing to the strong avidin/biotin interaction. The wisdom behind these choices is to start from readily available nanomaterials to avoid the tedious synthesis, separation, and characterization of steps of nanomaterials. Furthermore, this approach will provide more reproducible results that are easy to translate into commercial devices. The reporter probes target 24-nt sequences located near the S and N genes (Figure 1A). They were functionalized with HRP using the readily available HRP conjugation kit and can be used without any purification step. The use of two reporter probes is intended to increase the fluorescence readout to improve the assay sensibility. Overall, the magnetic capture probes were first used to extract the viral RNA from the whole RNA mixture purified from the collected human nasopharyngeal swabs (Figure 1B). Once magnetically separated from the rest of human RNA (b), the viral RNA was hybridized with the reporter probes. Excess of the reporters were later washed out. Finally, solutions of hydrogen peroxide and OPD were simultaneously added to detect the HRP-induced DAP fluorescence. It is worth noting that HRP has been shown to have a turnover number of ca. 530−750 s^{-1},[20] leading to the production of a large number of fluorescent molecules in a few minutes, thus giving rise to high fluorescence readout in a short time.

Optimization of the Operational Parameters. Several factors that influence the analytical performances of the developed bioassay have been optimized. The examined ranges for each parameter and their optimum values are gathered in Table 1. All variables were optimized using the largest signal-to-noise ratio (S/N) as a selection criterion. We first evaluated the effect of the amounts of magnetic beads (MBs) on the analytical response in the range from 0.1 to 1 mg/mL. As shown in Figure 2A, the highest S/N ratio was achieved with a concentration of 0.4 mg/mL and then decreased for higher concentrations. This may be due to the steric hindrance of the biomodified MBs, which limits the hybridization efficiency with the target RNA, leading to a lower fluorescence. Thus, 0.4 mg/mL was selected for the subsequent experiments.

Next, we examined the effect of the capture probe concentration ranging from 0.01 to 1 μM (Figure 2B). Data showed 0.05 μM as the optimal concentration, while for the control experiment, a direct correlation between the fluorescence and the probe concentration was found, suggesting that nonspecific adsorption was favored by a higher concentration of the capture probe. We have further optimized the incubation time with the target RNA, since time is an important parameter for the hybridization process. As depicted in Figure 2C, the largest S/N ratio was obtained for a duration of 10−15 min, which was then selected as the hybridization time.

Table 1. Ranges for the Examined Parameters and the Selected Values Based on the Intensity of the Fluorescence Readout and the S/N Ratio

parameters	ranges	selected values
magnetic beads	0.1−1.0 mg/mL	0.4
capture probe	0.01−1.0 μM	0.05
incubation time with the capture probes	10−30 min	15
number of steps	1 or 2	2
reporter probe dilution ratio	1/50−1/1000	1/250
incubation time with the reporter probes	15−45 min	20 min
ionic strength (NaCl concentration)	0.1−1.0 M	0.8 M

The number of steps was also evaluated to simplify the whole working protocol and the turnaround assay time. We examined a one-step protocol where the target RNA was mixed with both the capture and reporter probes, followed by the fluorescence readout. In the two-step protocol, the target was first incubated with the capture probe, and after the magnetic extraction, the RNA was hybridized with the HRP-conjugated probe. The results clearly showed a better performance by the two-step protocol that produced a larger S/N ratio. This suggests a decrease of the hybridization process efficiency when simultaneous incubation with the capture and reporter probes is performed (Figure 2F). Afterward, the effect of the dilution of the HRP-conjugated reporter was examined. As displayed in Figure 2D, 1/250 dilution resulted in the highest fluorescence and the largest S/N ratio. Above 1/250, the fluorescence sharply decreased, probably caused by lower hybridization levels when low concentrations of the reporter were used. Next, the incubation time with the reporter was assayed. The highest S/N ratio was achieved in 15−20 min (Figure 2E). Accordingly, this incubation time ensured an efficient hybridization with the immobilized heteroduplexes and was selected for further experiments.

The influence of the hybridization buffer was also evaluated since ionic strength is one of the most relevant factors in DNA hybridization and immobilization efficiency.[21] To study this variable, hybridization was performed in saline−sodium citrate buffer (pH 7.5) with different concentrations of NaCl ranging from 0.1 to 1 M. The signal increased up to 0.8 M NaCl (Figure 2G), confirming the effect of salt ions on the enhancement of hybridization efficiency. In fact, sodium ions are attracted to the negatively charged phosphate backbone of the RNA, decreasing the electrostatic repulsion between strands and consequently enhancing the hybridization process. Therefore, NaCl at 0.8 M was chosen for the subsequent studies.

Simultaneous versus Subsequent Use of the Probes. It is crucial to evaluate the use of several extractions and reporting probes targeting several positions on the viral RNA. This would help us verify whether the simultaneous immobilization of both capture probes will have any competition-related problems that could compromise the

https://doi.org/10.1021/acs.analchem.1c01950
Anal. Chem. 2021, 93, 11225−11232

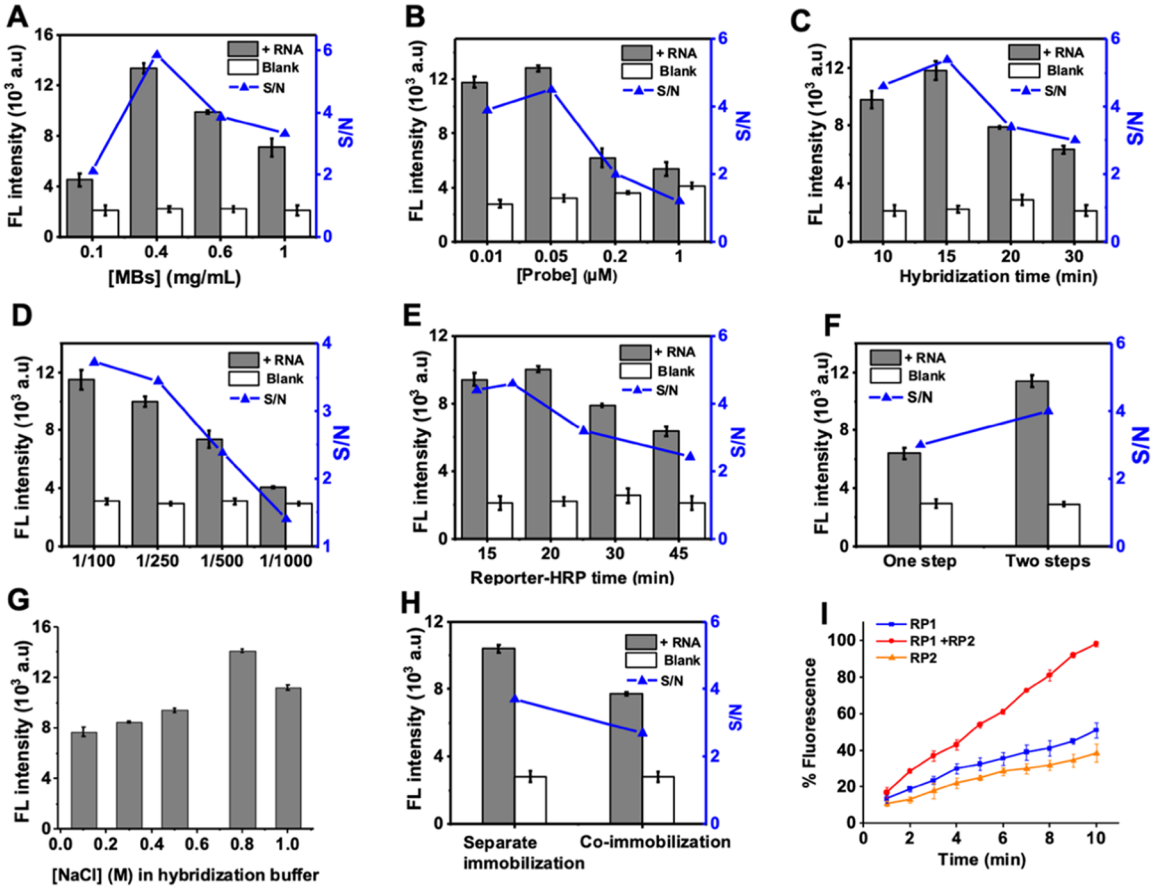

Figure 2. Display of the optimization of the influential parameters governing the assay. Optimization of (A) the concentration of MBs. (B, C) Concentration of the capture probe and its hybridization time. (D, E) Dilution factor of the HRP-conjugated DNA probe and its hybridization time. (F) Number of steps in the protocol and the number of steps performed in the hybridization procedure. (G) Effect of NaCl concentration in the hybridization buffer. (H) Comparison of the response obtained after co-immobilization and separate immobilization of the capture probes. (I) RP1 and RP2 tested individually and in combination with the two reporter probes using 10 min assay time. The percentage of fluorescence is calculated using the following formula, %FL = $(F/F_0) \times 100$. The standard deviations of measurements were performed from three independent replicates.

analytical response. In the first experiment, the two capture probes were separately immobilized on the magnetic beads and subsequently the two suspensions were mixed together to extract the target RNA, while in the second experiment, concomitant tethering of the two probes on the same magnetic beads was carried out for the sake of comparison. As shown in Figure 2H, the S/N ratio was 20% higher in the case of separate coupling of each probe on the MBs compared to the co-immobilization method. These results may be explained by the competition that took place between the sequences. Regardless of these findings, co-immobilization displays better characteristics in terms of reduced time assay, reagent consumption, and simplicity of the procedure, leading us to choose it over the method with separate probes.

Furthermore, we examined the effect of using two reporter probes, instead of one, on the signal intensity. Using 10 min assay time to avoid the saturation of the readout signal, we found that the use of both reporters produced a signal twice as high as that produced by the use of one probe (Figure 2I), which is in agreement with the literature.[14] The use of two probes will allow lowering the detection limit and improving the sensitivity.

Analytical Performance. We evaluated the performance of our approach for detection of SARS-CoV-2 RNA using a dilution series of the total RNA from COVID-19-positive patients. The data showed an increase in fluorescence responses correlated with the different concentrations of the target RNA ranging from 0.02 to 3.0 ng/μL. The limit of detection was estimated to be 0.01 ng/μL (1×10^3 copies/μL) using the three times σ/s criterion, where σ corresponds to the standard deviation of the blank value and s is the sensitivity at low concentration, which corresponds to the slope value of the correlation curve (Figure 3A). Furthermore, we used two synthetic RNA sequences with one-mismatched base either in the capture probe zone or in the reporter probe zone to examine the single nucleotide polymorphism effect (Table S1). We noticed that the designed probes produced only a weak response, slightly higher than that of the control experiment, with the mutated synthetic RNA. This demonstrates the bioassay selectivity, which can be used to distinguish between the mutated and nonmutated strains of the virus (Figure 3B). In addition, we investigated the specificity against a panel of positive-sense RNA viruses such as hepatitis C, West Nile, measles, and non-polio enteroviruses (Figure 3C). Only the SARS-CoV-2 RNA produced a fluorescence response, indicating the high specificity of the developed assay. Bioinformatic analysis of the capture and reporter probes, using BLAST with other known members of the respiratory

https://doi.org/10.1021/acs.analchem.1c01950
Anal. Chem. 2021, 93, 11225−11232

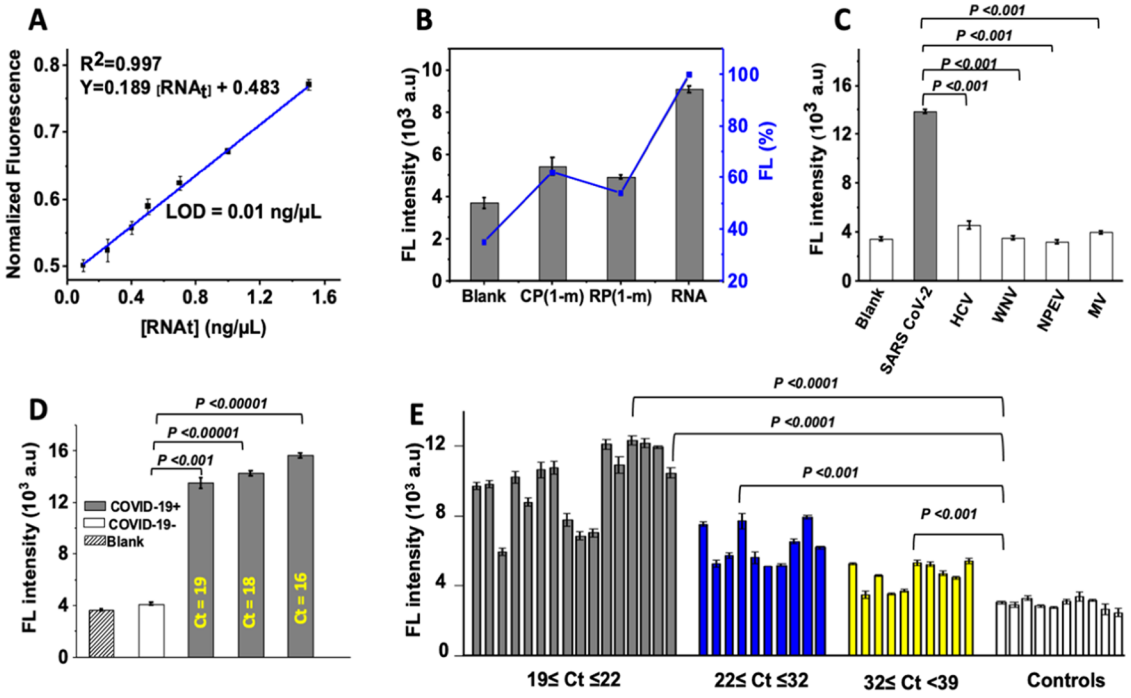

Figure 3. (A) Correlation between the fluorescence intensity and total RNA concentrations (0, 0.02, 0.1, 0.25, 0.4, 0.5, 0.7, 1, 1.5, 3 ng/μL). Error bars were estimated as triple the standard deviation (n = 3). (B) Selectivity test using one-mismatched base sequence in the capture or the reporter probe. (C) Selectivity test using a set of human RNA viruses. (D) Analysis of samples collected from the COVID-19-positive patients and COVID-19-negative subjects. Values of the C_t are indicated over the bar (P < 0.0001). (E) Clinical validation of the developed biosensor on RNA samples, purified from nasopharyngeal swabs of 46 human subjects (36 COVID-19-positive and 10 COVID-19-negative as assessed with RT-qPCR).

coronavirus family, namely, HCoV-NL63, HCoV-OC43, and HCoV-HKU1, showed limited similarities, thus demonstrating the potential selectivity of the bioassay.

Detecting the Viral RNA in Clinical Samples. All tested samples, prepared from nasopharyngeal swabs of SARS-CoV-2-positive patients, yielded positive results, while the negative clinical samples provided negative results (Figure 3D). A comparison of the fluorescence signals with the cycle threshold (C_t) values, obtained from RT-qPCR, exhibited a direct correlation. As expected, samples with lower C_t (i.e., containing high viral loads) produced higher fluorescence signals. Analysis of covariance (ANCOVA) provided P values less than 0.001, denoting high statistical significance.[22] Furthermore, to validate the bioassay, we used it to analyze 46 clinical samples (36 COVID-19-positive patients and 10 COVID-19-negative subjects, as assessed by RT-qPCR). Different sets of samples were chosen with low (19−22), intermediate (22−32), and high (32−39) cycle threshold values. ANCOVA for the different sets showed significant differences between positive and negative patients (P < 0.001), even for samples with the lowest viral load ($32 \leq C_t \leq 39$). The negative diagnosis, using RT-PCR, was set to a C_t value of 40.

The method sensitivity was determined from the ratio of the positive cases found by our method to the number of positive cases from RT-qPCR analysis. Similarly, the specificity was calculated as the ratio of negative cases from our method to those assessed by RT-qPCR. Both the sensitivity and the specificity were 100% for the set of analyzed samples. To the best of our knowledge, only a few works have examined the direct detection of the viral RNA without DNA/RNA thermal and isothermal amplification techniques. For the sake of comparison, in Table 2, we compiled the techniques, principles, dynamic ranges, and detection limits of the different types of recently reported amplification-free methods for SARS-CoV-2 detection. Our bioplatform shows acceptable results in terms of range of detection and detection limit. Furthermore, all of the work was carried out using real samples, and the platform was validated using a cohort of 36 COVID-19-positive patients and 10 COVID-19-negative controls.

DISCUSSION

In 2019, a new coronavirus strain, SARS-CoV-2, emerged in Wuhan (China) causing the current pandemic.[1] RT-qPCR quickly became the gold standard method to diagnose patients to take necessary steps to mitigate the outbreak. Due to shortages in reagents and the cumbersomeness of RT-PCR,[23] there is an urgent need for alternative amenable methods meeting the WHO ASSURED (affordable, sensitive, selective, user-friendly, rapid and robust, equipment-free, and deliverable to end-users) criteria.[24] Several researchers have devised RNA amplification-free approaches that skip the genetic material amplification using DNA primers.[12−14,25] Furthermore, RT-qPCR shows pitfalls, which are linked to the choice of amplification primers that can be totally unreliable such as the RdRp-SARSr primer by Charité Hospital of Berlin.[26]

Here, we show that the use of a combination of magnetic capture and reporter probes was effective in the amplification-free detection of SARS-CoV-2 RNA using fluorescence readout. This method offers a promising option for the quantitative, rapid, and point-of-care testing of COVID-19. Optimization of key parameters influencing the method showed that load of the probes, hybridization time with the target RNA, ionic strength of the buffer solution, etc., need to be adjusted to produce the highest signal-to-noise ratio, especially when the work is carried out using total RNA instead of buffered solutions spiked with in vitro transcription RNA.

https://doi.org/10.1021/acs.analchem.1c01950
Anal. Chem. 2021, 93, 11225−11232

Table 2. Nucleic Acid Amplification-Free Methods Designed for the Detection of SARS-CoV-2 Genetic Material and their Performances

technique	principle	dynamic range	detection limit	minimal assay time	real samples	references
optical	naked-eye detection of the viral RNA using four antisense oligonucleotides	0.2−3 ng/μL	0.18 ng/μL	10 min	nasopharyngeal swabs	12
electrochemical	electrochemical paper-based detection method of the viral RNA using up to four specific antisense oligonucleotides	5.85×10^2 to 5.85×10^7 copies/μL	6.9 copies/μL	5 min	nasopharyngeal swabs	13
CRISPR−Cas13a	amplification-free detection of the viral RNA with CRISPR−Cas13a and mobile phone microscopy readout	10^3 to 10^5 copies/μL	100 copies/μL	5−30 min	nasal swabs	14
lateral flow	amplification-free nucleic acid immunoassay, implemented on a lateral flow strip, with fluorescence detection of SARS-CoV-2 RNA	10^6 to 10^9 TU/μL	5×10^5 copies/μL	15 min	sputum and throat swabs	18
colorimetric fluorescence Raman (SERS)	a triple-mode bioplatform based on AuNPs for the fast and selective detection of viral RNA	160−1 nM	160 fM 259 fM 395 fM	40 min	throat swabs	19
fluorescence	magnetofluorescent amplification-free detection of the viral RNA from the total RNA using capture and HRP-conjugated reporting probes	0.01−3 ng/μL	1.02×10^3 copies/μL	25−30 min	nasal swabs	this work

Using one reporting probe allowed convenient detection of the viral RNA with a detection limit of 1×10^3 copies/μL. The second set of probes showed similar results, while combining the two sets improved the LOD by a factor ranging from 2.3 to 2.7 and the slopes from 3.80 to 3.23 a.u./min (individually to 8.85 a.u./min) (Figure 3E). This near tripling of the average slope, compared to the individual reactions, indicates the advantage of combining the two reporting probes. More reporters can be used to further improve the detection capability of the bioassay.

Furthermore, estimation of the cost of an experiment run in triplicate is less than $0.5, which is extremely useful to implant the bioassay in low-resource settings, airports, and for point-of-care (POC) testing. The sensitivity and specificity of the bioassay were estimated to be equal to 100% from the analysis of a cohort of samples collected from nasopharyngeal swabs of 46 human subjects (36 patients and 10 controls assessed with RT-qPCR), denoting the high accuracy of this method. The ANCOVA results showed that even real samples with high C_t values were clearly distinguished, by our device, from samples of negative subjects ($P < 0.001$). Finally, the magnetic capture and reporting probes were stable for a period of 45 days, when they were used on a daily basis, which avoids repetitive preparation of the bioreagents needed for the fluorometric assay.

This work reports a proof of concept for amplification-free, rapid, and sensitive detection of SARS-CoV-2 RNA using a combination of two capture and two reporter probes. Still, more investigations are needed to fully translate this concept into a viable point-of-care device. Moving toward clinical applications, our designed bioassay for the viral RNA detection overcomes some drawbacks of the already available methods on the market[13,14,19] to be able to fulfill the WHO ASSURED criteria. Indeed, we used extracted RNA, obtained using commercial RNA extraction kits, and an extraction-free protocol would drastically reduce the number of steps and the sample-to-answer turnaround time. This achievement is of great significance because extraction protocols usually require costly reagents and are complex. However, we used benchtop spectrofluorometers that could be replaced by cost-effective handheld devices, which are commercially available starting from US $500, allowing POC use in low-resource settings and at points of entry to a specific country.

Samples with $C_t > 38-40$ were not tested to examine the assay sensitivity in more detail. Finally, we demonstrated a detection limit of 1×10^3 copies/μL in 20 min, and we are currently working to improve this limit and increase the linear range using more than two capture and reporter probes and fluorogenic reagents with higher quantum yields and which provide good stability instead of OPD. It is noteworthy to mention fluorescent nanoparticle-based assays in comparison with our developed method. Several previous works have utilized quantum dots as highly fluorescent particles that have good biocompatibility and provide highly sensitive and specific detection. One key advantage with fluorescent particle-based assays is that they can be performed in one-step incubation without additional reagents and washing steps, thus simplifying the assay procedure for a shorter time. For example, Ren et al.[27] provide a good example of a novel strategy for miRNA detection based on fluorescence-enhanced protein p19-conjugated QDs. The proposed assay can sensitively detect as low as 0.6 fM miRNA-21 without any amplification techniques.

https://doi.org/10.1021/acs.analchem.1c01950
Anal. Chem. 2021, 93, 11225−11232

CONCLUSIONS

Diagnostic devices meeting the WHO ASSURED criteria are of paramount importance to provide a swift response to the ongoing and subsequent pandemics. In the present work, we report the design of a novel and sensitive magnetofluorescent bioassay to detect the viral RNA in total RNA samples collected from nasal swabs of COVID-19-positive patients without any RNA/DNA amplification step. The method uses antisense magnetic capture and HRP-labeled reporter oligonucleotides that recognize specific regions of the viral RNA. The assay can detect less than 1.02×10^3 copies/μL in the range from 1×10^3 to 9×10^7 copies/μL in less than 30 min. Selectivity of our device was better verified when challenged with several RNA positive-sense enteroviruses such as HCV, West Nile virus, measles virus, and non-polio enteroviruses. Furthermore, statistical analysis showed that the delivered response by device is different from COVID-19-positive patients compared to that from healthy control subjects. The assay was validated using a cohort of 46 clinical specimens of total RNA collected from COVID-19-positive patients and healthy subjects, showing that it has 100% sensitivity and specificity. The assay is modular and can be easily adapted to other variants of the virus and is inexpensive enough to be used in low-resource settings and for POC testing.

ASSOCIATED CONTENT

Supporting Information

The Supporting Information is available free of charge at https://pubs.acs.org/doi/10.1021/acs.analchem.1c01950.

Details about the experimental methods; DNA/RNA sequences used in this work as well as the sequences of the primers and probes used for the RT-PCR assay; and target-binding energies for capture and reporter probes (PDF)

AUTHOR INFORMATION

Corresponding Author

Noureddine Raouafi − *Sensors and Biosensors Group, Laboratory of Analytical Chemistry & Electrochemistry (LR99ES15), Faculty of Science, University of Tunis El Manar, 2092 Tunis, Tunisia;* orcid.org/0000-0001-8938-8221; Email: noureddine.raouafi@fst.utm.tn

Authors

Riham Zayani − *Sensors and Biosensors Group, Laboratory of Analytical Chemistry & Electrochemistry (LR99ES15), Faculty of Science, University of Tunis El Manar, 2092 Tunis, Tunisia*

Dorra Rezig − *Laboratory of Clinical Virology, WHO Reference Laboratory for Poliomyelitis and Measles in the Eastern Mediterranean Region, Pasteur Institute of Tunis, University of Tunis El Manar, 1068 Tunis, Tunisia; Research Laboratory "Virus, Vectors and Hosts: One Health Approach and Technological Innovation for a Better Health", LR20IPT02, Pasteur Institute of Tunis, 1006 Tunis, Tunisia*

Wasfi Fares − *Laboratory of Clinical Virology, WHO Reference Laboratory for Poliomyelitis and Measles in the Eastern Mediterranean Region, Pasteur Institute of Tunis, University of Tunis El Manar, 1068 Tunis, Tunisia; Research Laboratory "Virus, Vectors and Hosts: One Health Approach and Technological Innovation for a Better Health", LR20IPT02, Pasteur Institute of Tunis, 1006 Tunis, Tunisia*

Mouna Marrakchi − *Sensors and Biosensors Group, Laboratory of Analytical Chemistry & Electrochemistry (LR99ES15), Faculty of Science, University of Tunis El Manar, 2092 Tunis, Tunisia*

Makram Essafi − *Laboratory Transmission, Control and Immunobiology of Infections (LTCII, LR11 IPT02), Pasteur Institute of Tunis, 1002 Tunis, Tunisia*

Complete contact information is available at: https://pubs.acs.org/10.1021/acs.analchem.1c01950

Notes

The authors declare no competing financial interest.

The studies involving human participants were reviewed and approved by the institutional ethics committee of Pasteur Institute of Tunis.

ACKNOWLEDGMENTS

The authors acknowledge the financial support from the Tunisian Ministry of Higher Education and Scientific Research through the PRF program for the SmartBioSens (ref: PRFCOV19-D2P2) and COVID-PP (ref: PRFCOV19-D3P1) projects.

REFERENCES

(1) Zhu, N.; Zhang, D.; Wang, W.; Li, X.; Yang, B.; Song, J.; Zhao, X.; Huang, B.; Shi, W.; Lu, R.; Niu, P.; Zhan, F.; Ma, X.; Wang, D.; Xu, W.; Wu, G.; Gao, G. F.; Tan, W.; et al. *N. Engl. J. Med.* **2020**, *382*, 727−733.

(2) World Health Organization. *Weekly Epidemiological Update*; World Health Organization: Geneva, 2021.

(3) Looi, M.-K. *Br. Med. J.* **2020**, *371*, No. m4113.

(4) O'Dowd, A. *Br. Med. J.* **2020**, *371*, No. m4832.

(5) Hou, Y. J.; Chiba, S.; Halfmann, P.; Ehre, C.; Kuroda, M.; Dinnon, K. H., 3rd; Leist, S. R.; Schafer, A.; Nakajima, N.; Takahashi, K.; Lee, R. E.; Mascenik, T. M.; Graham, R.; Edwards, C. E.; Tse, L. V.; Okuda, K.; Markmann, A. J.; Bartelt, L.; de Silva, A.; Margolis, D. M.; Boucher, R. C.; Randell, S. H.; Suzuki, T.; Gralinski, L. E.; Kawaoka, Y.; Baric, R. S. *Science* **2020**, *370*, No. eabe8499.

(6) Gu, H.; Chen, Q.; Yang, G.; He, L.; Fan, H.; Deng, Y.-Q.; Wang, Y.; Teng, Y.; Zhao, Z.; Cui, Y.; Li, Y.; Li, X.-F.; Li, J.; Zhang, N.-N.; Yang, X.; Chen, S.; Guo, Y.; Zhao, G.; Wang, X.; Luo, D.-Y.; Wang, H.; Yang, X.; Li, Y.; Han, G.; He, Y.; Zhou, X.; Geng, S.; Sheng, X.; Jiang, S.; Sun, S.; Qin, C.-F.; Zhou, Y. *Science* **2020**, *369*, 1603−1607.

(7) Challen, R.; Brooks-Pollock, E.; Read, J. M.; Dyson, L.; Tsaneva-Atanasova, K.; Danon, L. *BMJ* **2021**, *372*, No. n579.

(8) Vandenberg, O.; Martiny, D.; Rochas, O.; van Belkum, A.; Kozlakidis, Z. *Nat. Rev. Microbiol.* **2021**, *19*, 171−183.

(9) Phua, J.; Weng, L.; Ling, L.; Egi, M.; Lim, C. M.; Divatia, J. V.; Shrestha, B. R.; Arabi, Y. M.; Ng, J.; Gomersall, C. D.; Nishimura, M.; Koh, Y.; Du, B.; Asian Critical Care Clinical Trials Group. *Lancet Respir. Med.* **2020**, *8*, 506−517.

(10) Santiago, I. *ChemBioChem* **2020**, *21*, 2880−2889.

(11) Bhalla, N.; Pan, Y. W.; Yang, Z. G.; Payam, A. F. *ACS Nano* **2020**, *14*, 7783−7807.

(12) Moitra, P.; Alafeef, M.; Dighe, K.; Frieman, M. B.; Pan, D. *ACS Nano* **2020**, *14*, 7617−7627.

(13) Alafeef, M.; Dighe, K.; Moitra, P.; Pan, D. *ACS Nano* **2020**, *14*, 17028−17045.

(14) Fozouni, P.; Son, S.; Díaz de León Derby, M.; Knott, G. J.; Gray, C. N.; D'Ambrosio, M. V.; Zhao, C.; Switz, N. A.; Kumar, G. R.; Stephens, S. I.; Boehm, D.; Tsou, C.-L.; Shu, J.; Bhuiya, A.; Armstrong, M.; Harris, A. R.; Chen, P.-Y.; Osterloh, J. M.; Meyer-Franke, A.; Joehnk, B.; Walcott, K.; Sil, A.; Langelier, C.; Pollard, K.

S.; Crawford, E. D.; Puschnik, A. S.; Phelps, M.; Kistler, A.; DeRisi, J. L.; Doudna, J. A.; Fletcher, D. A.; Ott, M. *Cell* **2021**, *184*, 323−333.
(15) Moshe, M.; Daunt, A.; Flower, B.; Simmons, B.; Brown, J. C.; Frise, R.; Penn, R.; Kugathasan, R.; Petersen, C.; Stockmann, H.; Ashby, D.; Riley, S.; Atchison, C.; Taylor, G. P.; Satkunarajah, S.; Naar, L.; Klaber, R.; Badhan, A.; Rosadas, C.; Marchesin, F.; Fernandez, N.; Sureda-Vives, M.; Cheeseman, H.; O'Hara, J.; Shattock, R.; Fontana, G.; Pallett, S. J. C.; Rayment, M.; Jones, R.; Moore, L. S. P.; Ashrafian, H.; Cherapanov, P.; Tedder, R.; McClure, M.; Ward, H.; Darzi, A.; Elliott, P.; Cooke, G. S.; Barclay, W. S.; On Behalf of the React Study Team. *Br. Med. J.* **2021**, *372*, No. n423.
(16) Li, Z. T.; Yi, Y. X.; Luo, X. M.; Xiong, N.; Liu, Y.; Li, S. Q.; Sun, R. L.; Wang, Y. Q.; Hu, B. C.; Chen, W.; Zhang, Y. C.; Wang, J.; Huang, B. F.; Lin, Y.; Yang, J. S.; Cai, W. S.; Wang, X. F.; Cheng, J.; Chen, Z. Q.; Sun, K. J.; Pan, W. M.; Zhan, Z. F.; Chen, L. Y.; Ye, F. *J. Med. Virol.* **2020**, *92*, 1518−1524.
(17) Nicol, T.; Lefeuvre, C.; Serri, O.; Pivert, A.; Joubaud, F.; Dubee, V.; Kouatchet, A.; Ducancelle, A.; Lunel-Fabiani, F.; Le Guillou-Guillemette, H. *J. Clin. Virol.* **2020**, *129*, No. 104511.
(18) Wang, D.; He, S.; Wang, X.; Yan, Y.; Liu, J.; Wu, S.; Liu, S.; Lei, Y.; Chen, M.; Li, L.; Zhang, J.; Zhang, L.; Hu, X.; Zheng, X.; Bai, J.; Zhang, Y.; Zhang, Y.; Song, M.; Tang, Y. *Nat. Biomed. Eng.* **2020**, *4*, 1150−1158.
(19) Gao, Y.; Han, Y.; Wang, C.; Qiang, L.; Gao, J.; Wang, Y.; Liu, H.; Han, L.; Zhang, Y. *Anal. Chim. Acta* **2021**, *1154*, No. 338330.
(20) Rani, D. N.; Abraham, T. E. *Appl. Biochem. Biotechnol.* **2006**, *128*, 215−226.
(21) Qiao, W. Q.; Chiang, H. C.; Xie, H.; Levicky, R. *Chem. Commun.* **2015**, *51*, 17245−17248.
(22) Concato, J.; Hartigan, J. A. *J. Invest. Med.* **2016**, *64*, 1166−1171.
(23) Chen, X. M.; Chen, Y. H.; Liu, C. G.; Li, X. J.; Liu, H. Y.; Yin, X. C.; Bai, X. F.; Ge, M.; Chen, H. Y.; Liu, M.; Du, Y. Z.; Fan, G. C.; Zhang, Y. *PLoS One* **2019**, *14*, No. e0219750.
(24) Kosack, C. S.; Page, A. L.; Klatser, P. R. *Bull. W. H. O.* **2017**, *95*, 639−645.
(25) Zhou, L. F.; Chandrasekaran, A. R.; Punnoose, J. A.; Bonenfant, G.; Charles, S.; Levchenko, O.; Badu, P.; Cavaliere, C.; Pager, C. T.; Halvorsen, K. *Sci. Adv.* **2020**, *6*, No. eabc6246.
(26) Vogels, C. B. F.; Brito, A. F.; Wyllie, A. L.; Fauver, J. R.; Ott, I. M.; Kalinich, C. C.; Petrone, M. E.; Casanovas-Massana, A.; Muenker, M. C.; Moore, A. J.; Klein, J.; Lu, P. W.; Lu-Culligan, A.; Jiang, X. D.; Kim, D. J.; Kudo, E.; Mao, T. Y.; Moriyama, M.; Oh, J. E.; Park, A.; Silva, J.; Song, E.; Takahashi, T.; Taura, M.; Tokuyama, M.; Venkataraman, A.; Weizman, O. E.; Wong, P.; Yang, Y. X.; Cheemarla, N. R.; White, E. B.; Lapidus, S.; Earnest, R.; Geng, B.; Vijayakumar, P.; Odio, C.; Fournier, J.; Bermejo, S.; Farhadian, S.; Dela Cruz, C. S.; Iwasaki, A.; Ko, A. I.; Landry, M. L.; Foxman, E. F.; Grubaugh, N. D. *Nat. Microbiol.* **2020**, *5*, 1299−1305.
(27) Ren, X.; Xue, Q.; Wen, L.; Li, X.; Wang, H. *Anal. Chim. Acta* **2019**, *1053*, 114−121.

https://doi.org/10.1021/acs.analchem.1c01950
Anal. Chem. 2021, 93, 11225−11232